Theoretical and Experimental Study of a Forward Swept Wing

Dr. Ibtisam A. Hassan
The University of Technology

Dr. A. S. Darwish
The University of Technology

Hayder M. Jaffal
The University of Mustansiriyah

Received on : 15/2/2010 **Accepted on : 8/12/2010**

Abstract

The aerodynamic characteristics of forward swept wing were studied theoretically and experimentally .In the present work, theoretically a computer program was constructed to predict the pressure distribution about surface of the wing using three dimensional Low Order Subsonic Panel method. The aerodynamic coefficients of the wing were calculated from the pressure distribution which gained from tangential velocities Experimentally ,test were carried out by designing and manufacturing a wing model with special arrangement for pressure tapping, suitable for low wind tunnel testing. The entire wing was rotated rotate about an axis in the plane of symmetry and normal to the chord to produce different sweep and incidence angles for wing, by using rotating mechanism. Wind tunnel test was carried out at ($U\infty$=33.23m/s) for different swept angles and angles of attack.

Comparisons were made between the predicted and experimental results. It is good and gave reasonable closeness. It was clear from the present investigation that the lift and drag characteristics for the forward swept wing are less in values compared with the swept back wing, therefore a forward swept wing can fly at higher speed corresponding to a pressure distribution associated for lower speed.

key words: Forward, Swept angles , Wing, **Aerodynamic characteristics.**

1. Introduction.

Before world war II, there were some gliders with forward swept wing, potential benefits identified for this technology include [1 , 2] :

1. Improve low speed aircraft handling characteristics.
2. Increased resistance to span\ departure .
3. Reduced aircraft stall speed .

Since sweep produces effects that vary with cos(sweep), the same result may be yield, with high speeds in the high subsonic Mach number region beginning to be attainable, aerodynamic designers found that sweeping wing either forward or aft delayed the rapid increase of transonic drag to higher Mach numbers [3,4] .

Some studies have examined the aerodynamic characteristics of forward swept wing and prove number the identical transonic maneuver design conditions, a forward swept wing can be provide lesser drag than an equivalent aft swept wing [5,6].

For laminar flow wing, the reduction in sweep in the case of forward swept wing leads to more stable laminar boundary layer concerning transition because of cross flow instability and attachment line transition [2,7] .

The use of forward swept wings has aerodynamic benefits at high angles of incidence and in supersonic regimes. These consist of reduction in wave drag, profile drag, and increased high angle of incidence handling qualities. These increased benefits are often offset due to an increase in structural components, to overcome flutter and wing tip divergence due to high loading of the wing tips at high angles of incidence [8] , as example for X-29 a forward swept wing flight research aircraft flight envelope was expanded to 66° angle of incidence [9].

The purpose of the present investigation is to introduce another point of view of the aerodynamic behavior of infinite forward swept wing theoretically by using low order panel method and compare the results with experimental tests on an isolated, stationary wing of an untwisted rectangular with different angles of sweep in low subsonic wind tunnel .

2. Theoretical Considerations:

Potential three-dimensional subsonic, irrotational, adiabatic and incompressible flow over any immersed body, has been investigated using low order panel method technique. Laplace equation solved for distribution singularities of constant strength source and doublet on each panel. The solution leads to calculate the strength of sources and doublets.

The total potential by using Laplace eq. may be written as:

$$\Phi^*_{xx} + \Phi^*_{yy} + \Phi^*_{zz} = 0 \qquad (1)$$

ϕ^* : includes potential of free stream and potential of perturbation which presented strength of singularities (source and doublet) :

$$\Phi^* = \Phi_\infty + \Phi \qquad (2)$$

ϕ : represented potential of perturbation, for incompressible flow :

$$\Phi_{xx} + \Phi_{yy} + \Phi_{zz} = 0 \qquad (3)$$

General solution of Laplace equation (1) can be determined using Green's identity for the distribution of source and doublet in three – dimensional flow [10] :

$$\Phi^*_{(x,y,z)} = -\frac{1}{4\pi}\int_s \left[\sigma\left[\frac{1}{r}\right] - \mu.n.\nabla\left[\frac{1}{r}\right]\right] ds + \Phi_\infty \qquad (4)$$

r : calculated as :

$$r = [(x-x_k)^2 + (y-y_k)^2 + (z-z_k)^2]^{1/2}$$

Where k = 1, 2, 3, 4

By using Drichlet boundary condition inside the body :

$$\Phi^*_i = constant = \Phi_\infty \qquad (5)$$

Putting potential inside the body ϕ_i equal to constant potential ϕ_∞, eq.(4) inside the body become :

$$\Phi_i(x,y,z) = \frac{1}{4\pi}\int_{body+wake} \mu.n.\nabla\left(\frac{1}{r}\right) ds - \frac{1}{4\pi}\int_{body} \sigma\left(\frac{1}{r}\right) ds + \Phi_\infty = \Phi_\infty \qquad (6)$$

and

$$\frac{1}{4\pi}\int_{body+wake} \mu.n.\nabla\left(\frac{1}{r}\right) ds - \frac{1}{4\pi}\int_{body} \sigma\left(\frac{1}{r}\right) ds = 0.0 \qquad (7)$$

Equation (7) is applied inside the body and wake.

After dividing the body into number of panels as shown in **Fig.(1A)** and transform the corner point for reference coordinate system as shown in **Fig.(1B)** the panel became as a flat plate.

Numerically eq. (7) on each control point may be written as [ref.(11)] :

$$\sum_{j=1}^{N_{t+w}} \frac{1}{4\pi} \int_{p} \mu_j \left[\bar{n}_t . \nabla \frac{1}{r_{jp}} \right] ds - \sum_{j=1}^{N_t} \frac{1}{4\pi} \int_{p} \sigma_j \left[\frac{1}{r_{jp}} \right] ds = 0 \qquad (8)$$

Where B_{jp} influence coefficient due to source

$$-\frac{1}{4\pi} \int_{1,2,3,4} \left(\frac{1}{r_{jp}} \right) ds = B_{jp} \qquad (9)$$

C_{jp} influence coefficient due to source.

$$\frac{1}{4\pi} \int_{1,2,3,4} \bar{n}_p \, . \nabla \left(\frac{1}{r_{jp}} \right) ds = C_{jp} \qquad (10)$$

The constant strength of source on each control point can be calculated by assuming normal component of velocity on surface of body equal to zero :

$$\bar{\sigma}_p = -U_\infty . \bar{n} \qquad (11)$$

In eq.(8) only strength of doublet μ_j is unknown and it can calculated by solving the set of equations numerically using Gausses elimination.

Finally tangentially velocity for each panel can be calculated and coefficient of pressure :

$$C_p = \frac{P_j - P_\infty}{\frac{1}{2}\rho_\infty U_\infty^2} = 1 - \left[\frac{U_j}{U_\infty} \right]^2 \qquad (12)$$

Coefficients of tangential and normal force on each control point for each panel are :

$$C_{zj} = C_{pj} A_j n_z \qquad (13)$$

$$C_{xj} = C_{pj} A_j n_x \qquad (14)$$

where

n_x , n_z :are normal vector components .

X_{cj} , Z_{cj} : are coordinates of control point .

A_j : is area of panel .

To calculate coefficient of lift and drag :

$$C_L = C_z \cos\alpha - C_x \sin\alpha \qquad (15)$$

$$C_D = C_z \sin\alpha - C_x \cos\alpha \qquad (16)$$

For this aim, a computer program was constructed in Fortran 77,see [ref(11)].

3. Experimental Work.

An open type, low speed wind tunnel is used for the present investigation with the following specification :

Cross - section working section $(305 * 305)\, mm^2$. Maximum air speed 36 m/s. overall dimension $3.9\ m * 1.1\ m * 1.6\ m$. power 6 kw. Fan speed 2900 rpm.

One half of full-span wing is tested in the wind tunnel. It has been standard practice in pressure distribution investigations in the Wind tunnel to make the assumption that there is no flow of air across the plane of symmetry of full-span wing. The further assumption follow that an actual surfaces(e.g. wind tunnel wall) may be located in this plane of symmetry without seriously affecting the air flow over either half of the wing, see **Fig(2)**. The general design of the wings' profile model and location of the static hole are shown in **Fig.(3).**The profile ordinates and static pressure tape location in part of chord (X/C) are given also in **Fig.(3)** .

The wing model is untwisted , rectangular wing with constant profile (type NASA 2415),thickness ratio (15%) tapper ratio equal to one, with a chord (150 mm) and span (210 mm).

The wing constructed from five pieces in span direction, four pieces with (40 mm) length and the fifth with (50 mm) length, where the static pressure tube are fixed in it. The five pieces are held together by the clamping action of two bolts. This method of assembly was necessary in order to allow us to take the pressure distribution in many spanwise location by changing the place of fifth piece. The wing has seventeen static pressure tap, ten on upper surface and seven on lower surface as shown in **Fig.(3)**, 1 mm in diameter and 0.8 mm in inner diameters, which they were connected by rubber tubing to a multiple manometer.

The wing was fixed in wind tunnel test section by two bolts , see **Fig. (2)**.

Sweep was obtained by loosening the mounting clamp, and rotating the entire wing (by mean of rotating mechanism stabilized in it) about an axis in the plane of symmetry and normal to the chord, as shown in **Fig.(2).**

A torque handle, extending out of the tunnel, which connected to the rotating mechanism, served as a means for changing the angle of incidence.

The mean dynamic pressure is measured at the working section by micro – digital manometer.

The experimental program for the wing was done as follows:

1- Straight wing.
2- Sweep forward, with quarter sweep angles $\left(\Lambda_{c/4} = 0^0 \rightarrow -45^\circ\ at\ increment\ of 5^\circ\right)$
3- Sweepback with quarter sweep angles $\left(\Lambda_{c/4} = 0^0 \rightarrow 45^\circ\ at\ increment\ of 5^\circ\right)$

Each test case tested at different angles of incidence between $(\alpha = -6^\circ \rightarrow 15^\circ\ at\ 3^0 step\ intervals)$. At each test case the conventional pressure – distribution being employed. The chord wise pressure distribution data were taken at span wise direction (y/b = 0.88, 0.61, 0.5, 0.33) from the root of wing. For more detailes see [ref (11)]. An air speed was maintained constant at $(\cup_\infty = 33.24 m/s)$ where Reynolds number based on the wing chord was kept about $(3.315 * 10^5)$. For all measured data corrections were applied ,according to [ref(12)], to the free stream velocity and to the force coefficients.

4.Results and Discussion.

The pressure data was collected from each port for different incidence and sweep angles at (Re $=3.315 * 10^5$). This experimental data was compared with Low Order Subsonic Panel method results.

A pressure coefficient distribution, along different y/b is represented in **Fig. (4)** .From this plot, it is clear that the C_p at (0.5 y/b) is initially higher (about 30%) than the C_p of tip regime (0.88 y/b).The increase in the C_p is due to the inward crossflow induced by vortices during the moderate lift region. Prior to stalling the airfoil, this difference in pressure coefficients, was almost be maximum at 40% of the root. Less than that, it will be diminished . A little disagreement between the numerical and an experimental C_p value distribution along the chordwise was shown in **Fig. (4)**. It was due to viscous effects, which Low Order Panel method is not capable of modeling. **Fig.(5)** shows a reasonable agreement between the present theoretical results (low order panel method) and the results obtained by [ref 6] which used the finite different method, (Pandora method).

The distribution of the pressure coefficient around the chordwise was represent in **Fig. (6)** and **Fig. (7)** for positive and negative incidence angles respectively at different forward-swept angles . As (+α) increases, which causes to increase the velocity on upper surface , the suction pressure will increase. While for the lower surface of wing, C_p distribution changes only mildly with incidence angle, in comparison with those on the upper surface. At (-α) ,the suction pressure will be overturned, as shown in **Fig. (7)**. It decreases at the upper surface and increase at the lower surface as the negative incident angle increase at the leading edge of the wing. The great influence of the leading edge position with respect to free stream velocity caused to change the sign of the suction pressure from negative at the positive incidence angle to positive at negative incidence angle. As the angle of sweep increases the suction pressure decrease. Maximum suction pressure was at an angle of sweep zero because, the wing was straight and the normal component of the velocity equal to free stream in this case which different with other cases.

Fig.(8) shows the lift curve slope angle along the spanwise location for sweep angles ($\Lambda_{c/4} = -10^\circ, -20^\circ$). Lift curves slope decreases as the spanwise location far from the root of wing ,refers to losses in lift toward the tip of the wing. It is expected to be zero at the edge because the energy of low transform to tip clearance vortices which increase the drag due to vortices. The reduction in lift curves slope caused by sweep clearly observed in **Fig. (8)** and **Fig. (9).**

A comparison between FSW and ASW experimental results, is presented in **Fig. (10)**. It shows that the lift coefficient for the forward swept wing is less than the lift coefficient for the aft swept wing at the same angle of incidence and the same spanwise location . e g. C_L at forward swept will reduced 21% than that of aft swept at $\Lambda_{c/4} = 10^\circ$ and 32% at $\Lambda_{c/4} = 40^\circ$ where $\alpha = 9^\circ$ and Y/b=0.69.

Fig. (11) presented the relation between C_L and C_D (experimental results) for different angles of attack and different swept angle at (y/b = 0.69), which shows that the C_D and C_L increase for FSW less than that for ASW.

Transition from sweepback to sweep forward increase the useful angle of incidence range. Sweep forward raise the angle of incidence of neutral stability and sweepback to lower it, relative to the angle for the straight wing. This effect seems to be due to the fact that the tip, which affect lateral stability more than any other part of the wing, act in manner analogous to the leading edge of an airfoil when swept forward and the trailing edge when swept back.

5. Conclusion.

Considering the forward sweep wings performance of the present work, the following concluded:

1. The aerodynamic characteristics for FSW are more stable at low speed, because the FSW provides a wide useful angle of incidence range.
2. The lift and drag coefficient diminish with an increase in forward and aft swept angles ,but it was less in forward swept angle.
3. The lift curve slope inclination decreases for the forward wing whenever increased sweeping, because:

$$\left.\frac{\partial c_L}{\partial \alpha}\right)_{\Lambda_{c/4}} = \left.\frac{\partial c_L}{\partial \alpha}\right)_{\Lambda=0} \cos(\Lambda_{c/4})$$

4. Lift curves slope decreases as the spanwise location far from the root of forward wing ,refers to losses in lift toward the tip of the wing because the energy of low transform to tip clearance vortices which increases the drag due to vortices.

6. References .

[1] German Aerospace Center (DLR), "Design of a Transonic Wing With Natural Laminar Flow for the EC project NACRE", KATnet II Drag Reduction Workshop 14th_16thOctober 2008 Ascot, UK.

[2] I. kroo, "Applied Aerodynamic Index "Stanford University 1996.

[3] Jhon J.Bertion & Michael L.Smith, "Aerodynamics for Engineers", Prentic – Hall 1998.

[4] S Siouris, N Qin, "Study of the effects of wing sweep on the performance of a blended wing body aircraft ",Journal of Aerospace Engineering, Volume 221, Number 1 / 2007.

.

[5] "X-29 Forward Swept Wing", NASA Dryden Flight Research Center, NASA : FS 98-04-008 DFRC, April, 1998.

[6] Micheal J.Mann & Charles E. Mercer, "Forward swept wing configuration Designed for High Maneuverability by use of a Transonic Computational Method", NASA Technical paper 2628, 1986.

[7] Redeke G. & Wichman , "Forward Swept a Favorable Concept for a Laminar Flow wing", Journal Aircraft Vol.28, No.2, February, 1991

[8] David W. R. "The Aerodynamic Analysis and Aero elastic Tailoring of a forward swept wing ", MSC. Thesis, Carolina State University, 2006.

[9] Trippensee, Gray "Update of the x-29 High Angel of Attack", program proceeding-society of Automotive Engineers n-p-246, pub by SAE Warrendal, PA, USA, 1991.

[10] Joseph, katz & Allen, poltion, "Low Speed Aerodynamics From Wing Theory to panel Method". Mc Graw-Hill, 1991.

[11] H. M. Jaffal, "Design Study of Aerodynamic Coefficients for the Forward Swept Wing", MSC Thesis, University of Technology, Baghdad, 2001.

[12] William H. R.& Alan P.," Low Speed Wind Tunnel" , John Wiley & Sons,1984

7. Nomenclature.

A_j	Area of panel (m^2)
ASW	Aft Swept Wing
b	Semispan of wing (mm)
C	Chord of wing (mm)
C_D	Drag coefficient due to pressure

C_L	Lift coefficient
C_P	Pressure coefficient
C_X	Tangential force coefficient
C_Z	Normal force coefficient
FSW	Forward Swept Wing
L	Number of panels in chordwise direction
M_∞	Free stream Mach number
N_t	Total number of panels
N_w	Number of panels in wake
N	Number of panels in spanwise direction
P_∞	Free stream pressure (N/m^2)
Re	Reynolds number
S	Surface area of wing (m^2)
U_i	Local panel Velocity (m/sec)
U_∞	Free stream velocity (m/sec)
y/b	Spanwise Location
X/C	Chordwise Location
α	Angle of incidence (deg.)
B	Compressibility correction factor
μ	Doublet strength (m^2/s)
σ	Source strength (m^2/s)
λ	Wing taper ratio, Tip chord/root chord
$\Lambda_{C/4}$	Quarter sweep angle (deg.)
$-\Lambda_{C/4}$	Forward sweep angle (deg.)
$+\Lambda_{C/4}$	Aft sweep angle (deg.)
ϕ^*	Total potential
ϕ_∞	Free stream potential
Φ	Potential of perturbation
x, y, z	Reference coordinates
η, ξ, ζ	Panel coordinates

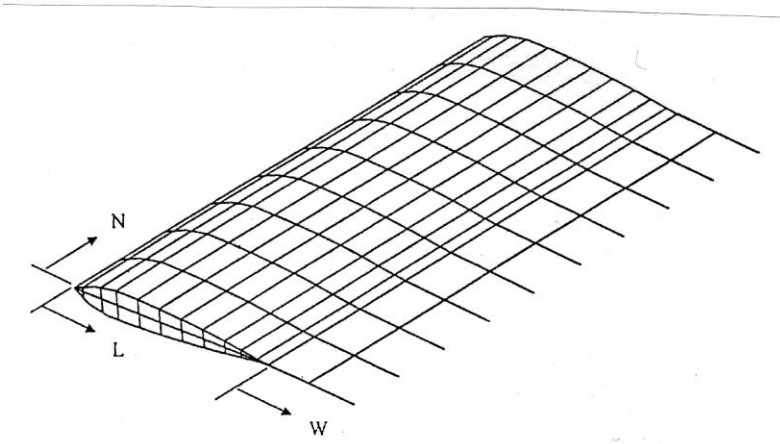

Fig.(1 A) Grid generation.

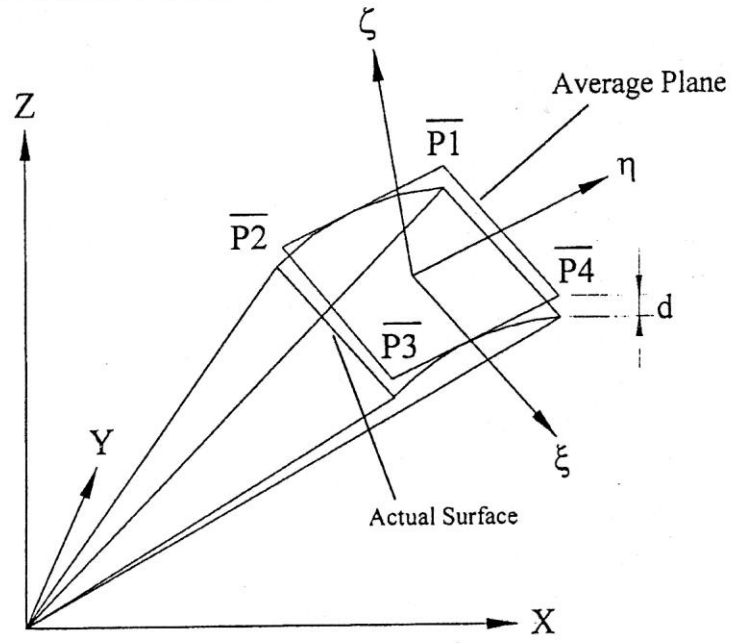

Fig.(1 B) Reference and average planes.

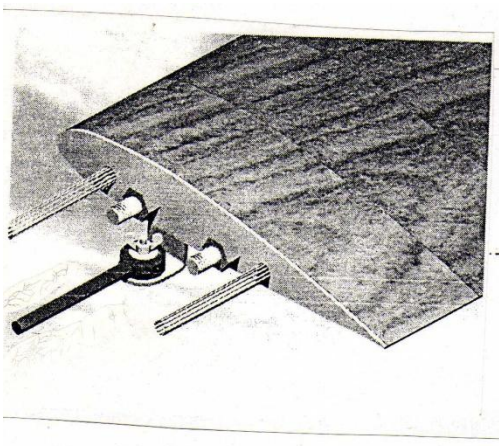

Fig. (2A) The manufacturing wing.

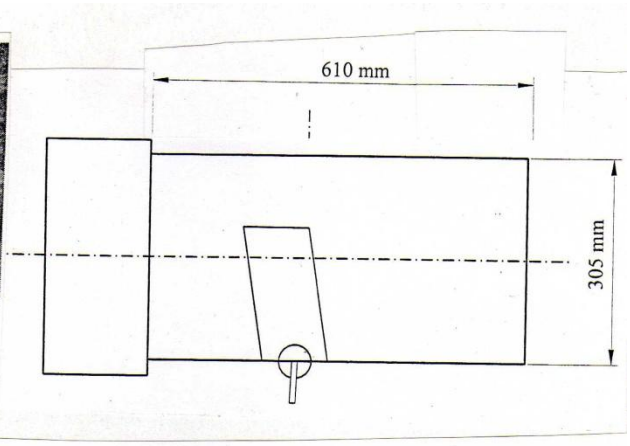

Fig (2B) Top view for test section Of wind tunnel.

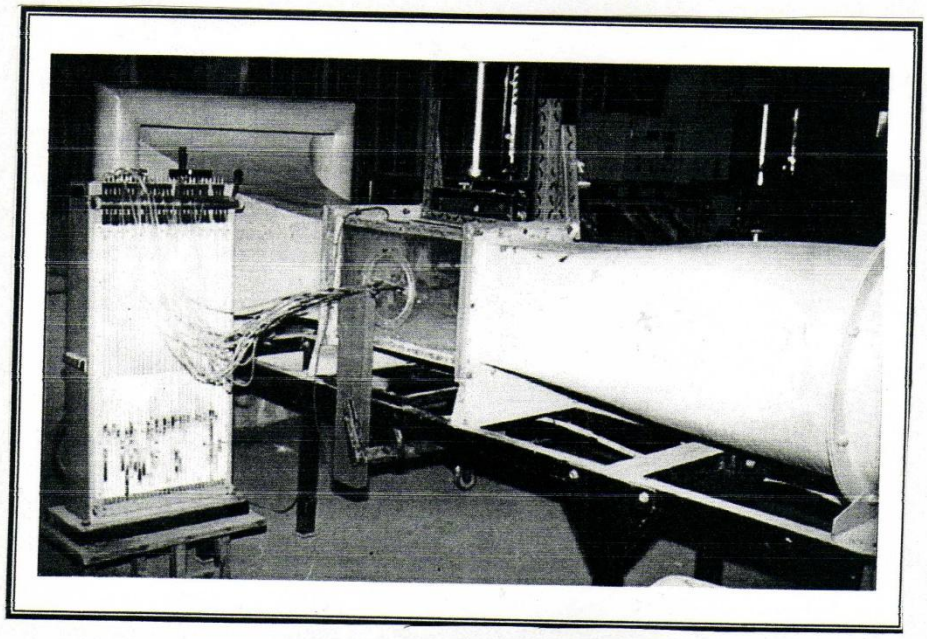

Fig.(2 C) Wing model mounted on wind tunnel .

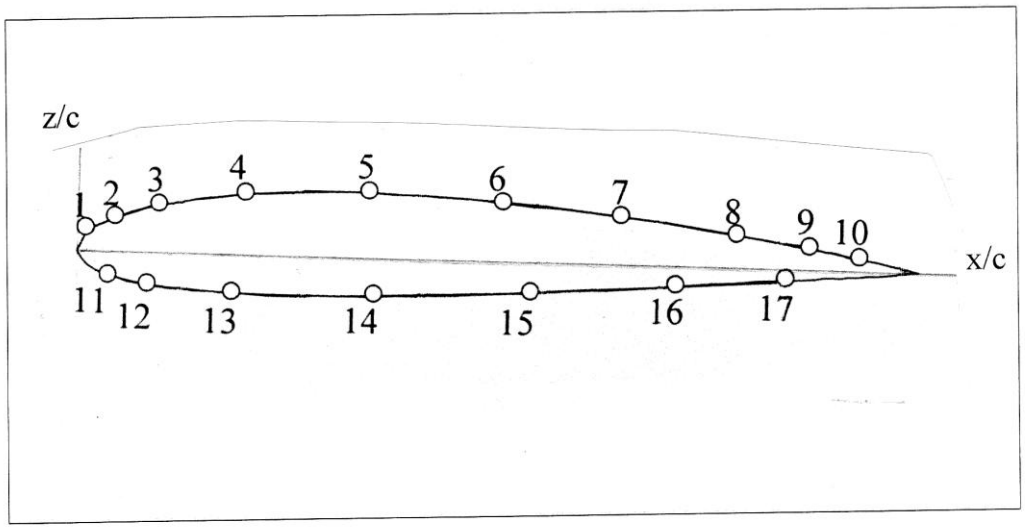

Pressure orifices location coordinates			Wing section coordinates(NACA 2415)		
z/c	x/c	No.	z/c (Lower)	z/c (Upper)	x/c
0.03	0.013333	1	0.0	0.0	0.0
0.049269	0.04666	2	-0.0206	0.0271	0.0125
0.06851	0.1	3	-0.0286	0.0371	0.025
0.087062	0.2	4	-0.0384	0.0507	0.05
0.094285	0.34666	5	-0.0447	0.0606	0.075
0.084546	0.50666	6	-0.049	0.0683	0.1
0.069212	0.64666	7	-0.0542	0.0797	0.15
0.047085	0.78666	8	-0.0566	0.087	0.2
0.029988	0.87333	9	-0.057	0.0917	0.25
0.016636	0.93333	10	-0.0562	0.0938	0.3
-0.03562	0.04	11	-0.0525	0.0925	0.4
-0.04688	0.08666	12	-0.048	0.0857	0.5
-0.05682	0.18666	13	-0.039	0.075	0.6
-0.05457	0.35333	14	-0.0305	0.061	0.7
-0.045	0.541	15	-0.0215	0.0441	0.8
-0.02957	0.71333	16	-0.0117	0.0245	0.9
-0.01695	0.84666	17	-0.0068	0.0134	0.95
			0.0	0.0	1.0

Fig.(3) The profile ordinates and orifices location in part of chord.

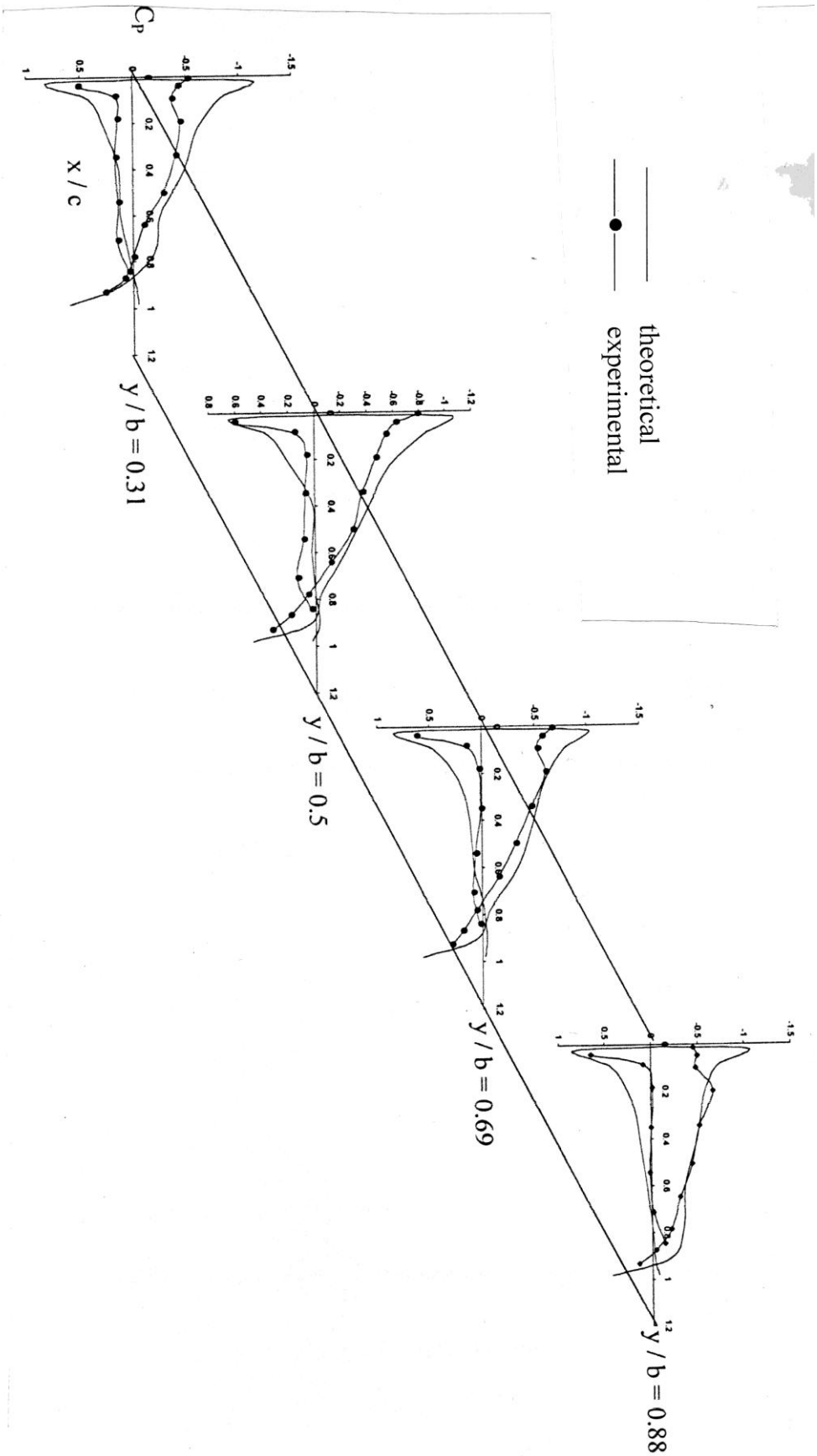

Fig.(4) Chordwise pressure distribution at different semispan location $\alpha = 6^0$, $\Lambda_{c/4} = -25^0$ (theoretical and experimental).

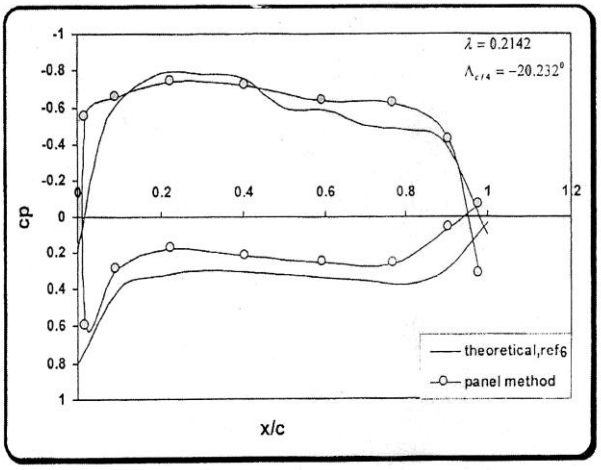

Fig.(5) Comparisons between present theoretical result and Ref.(6)

y/b = 0.65 , M = 0.85

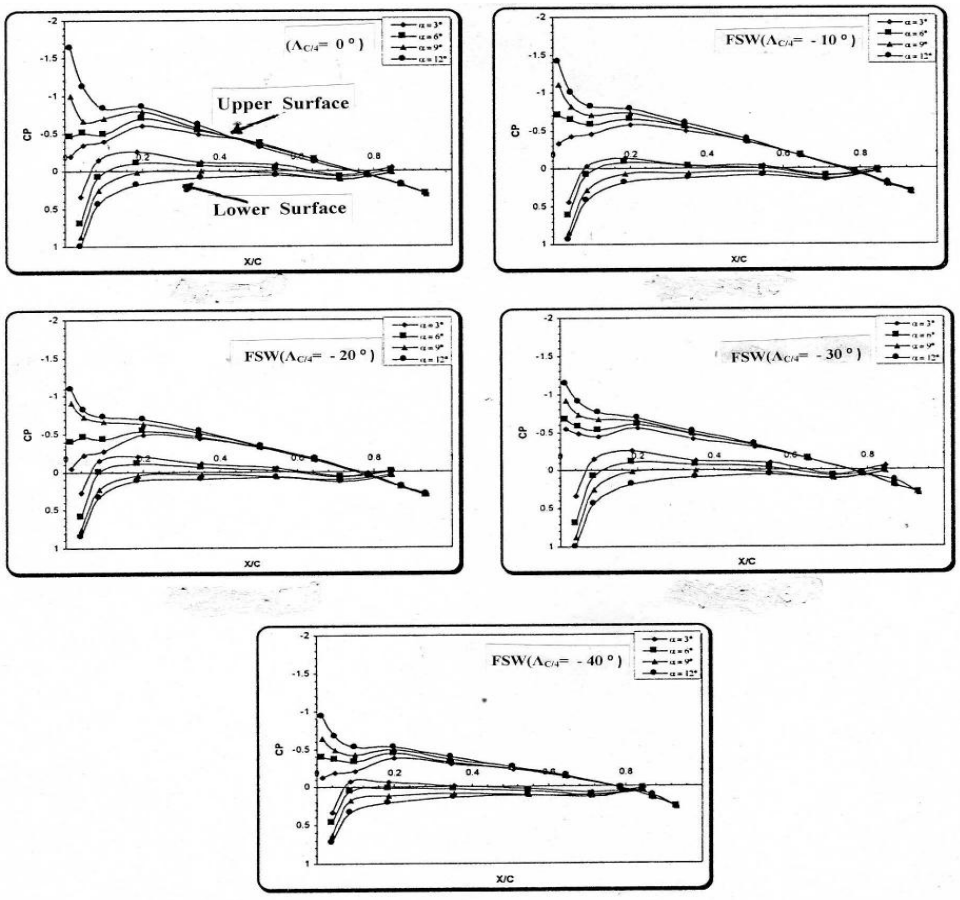

Fig.(6) Experimental chordwise pressure distribution of FSW for positive angle of incidence at y/b = 0.88.

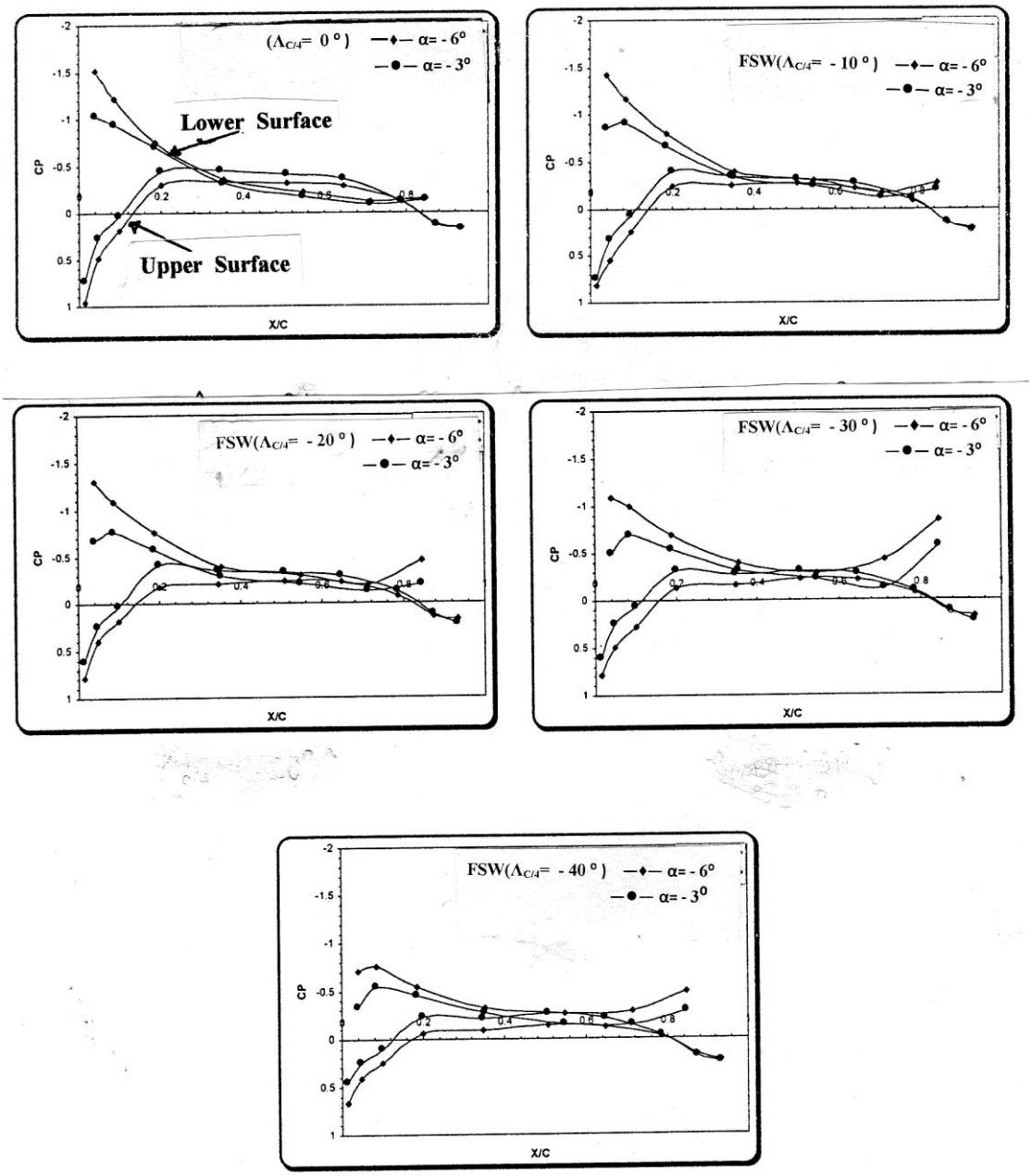

Fig.(7) Experimental chordwise pressure distribution of FSW for negative angle of incidence at y/b = 0.88.

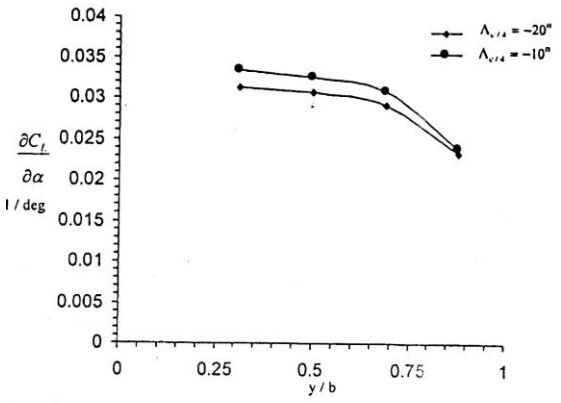

Fig.(8) Experimental lift curve slop along the spanwise location.

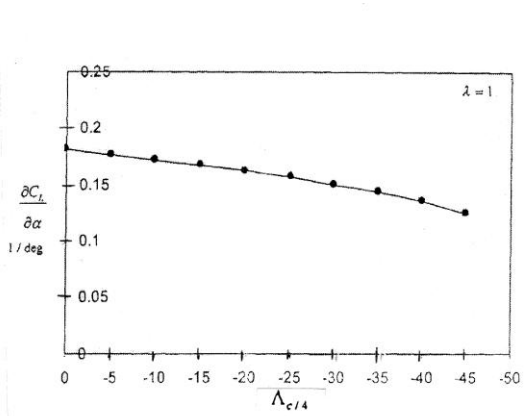

Fig.(9) Theoretical lift curve slop against sweep angle.

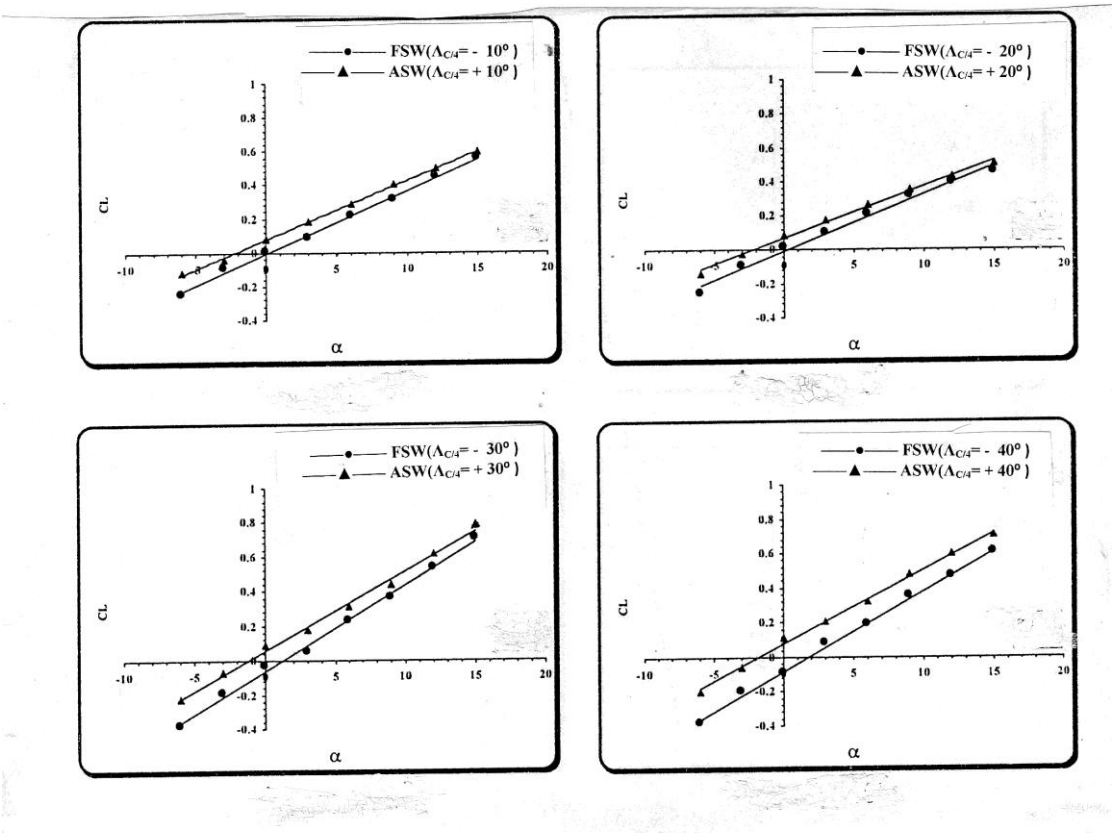

Fig.(10) Comparison between lift coefficient for FSW and ASW at y/b = 0.69 (experimental).

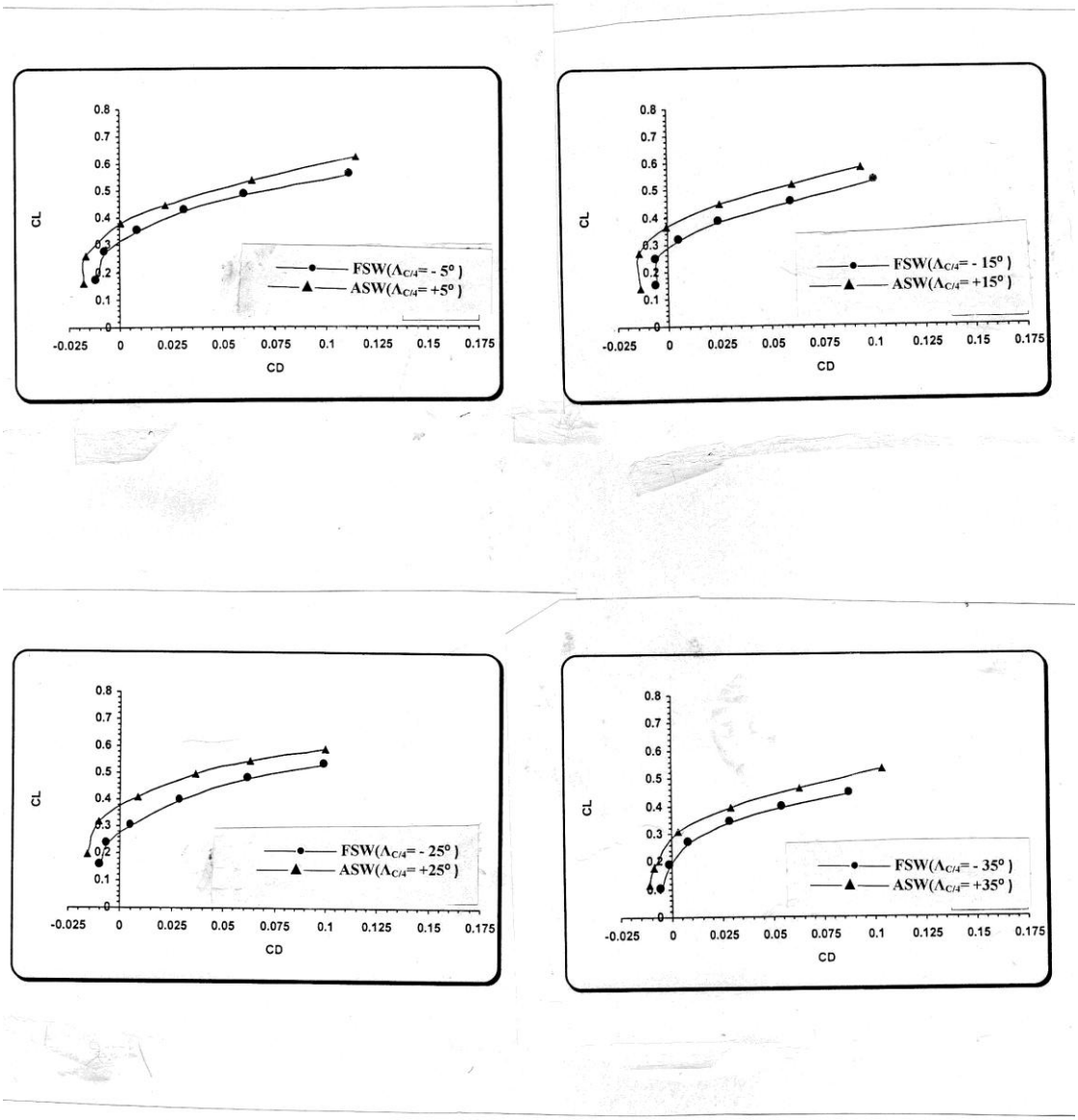

Fig. (11) The relation between C_L and C_D for different angles of incidence and different swept angles at y/b = 0.69 ,(experimental results)

دراسة عملية ونظرية لجناح ذات اكتساح متقدم

د٠ابتسام احمد حسن — الجامعة التكنولوجية
د٠ عبد السلام درويش — الجامعة التكنولوجية
المهندس حيدر محمد جفال — الجامعة المستنصرية

الخلاصة.

تم في هذا البحث دراسة الخصائص الديناهوائيه للجناح ذي الاكتساح المتقدم نظريا وعمليا. الدراسة النظرية تضمنت بناء برنامج حسابي تم فيه حساب توزيع الضغط على سطح جناح باستخدام طريقة الاشرطة ثلاثية الابعاد ذات الدرجة الواطئة.تم حساب السرعة المماسية ومنها حساب توزيع الضغط على سطح الجناح عند السرع تحت الصوتية ثم حساب المعاملات الديناهوائيه٠

عمليا ،تم تصميم وتصنيع نموذج لجناح ذي مقطع ثابت ٠اجريت مجموعة من التجارب المختبرية لذالك الجناح باستخدام نفق هوائى واطىء السرعة (U_∞=33.24 m/Sce)، مع الأخذ بنظر الاعتبار ادخال متغير اكتساح الجناح في تلك التجارب وقياس توزيع الضغط على سطح الجناح حول مقطعه وعلى مواقع مختلفة من الباع .

قورنت النتائج النظرية بتلك المناظرة لها المستخرجة من التجارب العملية، حيث اظهرت النتائج وجود توافق مقبول فيما بينها كما اظهرت انتائج التي تم التوصل اليها في هذه الدراسة ان خصائص الكبح والرفع للجناح المتقدم تكون اقل من الرفع والكبح للجناح المتراجع المناظر له ويمكن استخدام هذا الاستنتاج لتصميم جناح يطير بسرعة عالية ولكن بتوزيع ضغط يخص سرع واطئة٠